First-principles study of structural, electronic, and optical properties of cubic $InAs_xN_yP_{1-x-y}$ triangular quaternary alloys*

I Hattabi[1], A Abdiche[2,4,†], F Soyalp[3], R Moussa[4], R Riane[4], K Hadji[4], S Bin-Omran[5], and R Khenata[2,‡]

[1] *Laboratoire synthèse et Catalyse, Ibn Khaldoun Université of Tiaret, Tiaret* 14000, *Algeria*
[2] *Laboratoire de Physique Quantique et de Modélisation Mathématique (LPQ3M), Département de Technologie, Université de Mascara, Mascara* 29000, *Algeria*
[3] *Department of Physics, Faculty of Education, Yüzüncü Yıl University*, 65080 *Van, Turkey*
[4] *Science and Technology Département Ibn Khaldoun Université de Tiaret, Tiaret* 14000, *Algeria*
[5] *Department of Physics and Astronomy, College of Science, King Saud University, Riyadh* 11451, *Saudi Arabia*

(Received 15 July 2016; revised manuscript received 29 September 2016; published online 30 November 2016)

In this paper, we investigated the structural, electronic and optical properties of InAs, InN and InP binary compounds and their related ternary and quaternary alloys by using the full potential linearized augmented plane wave (FP-LAPW) method based on density functional theory (DFT). The total energies, the lattice parameters, and the bulk modulus and its first pressure derivative were calculated using different exchange correlation approximations. The local density approach (LDA) and Tran–Blaha modified Becke–Johnson (TB-mBJ) approximations were used to calculate the band structure. Nonlinear variations of the lattice parameters, the bulk modulus and the band gap with compositions x and y are found. Furthermore, the optical properties and the dielectric function, refractive index and loss energy were computed. Our results are in good agreement with the validated experimental and theoretical data found in the literature.

Keywords: density functional theory, full potential linearized augmented plane wave, Tran–Blaha modified Becke–Johnson approximations, $InAs_xN_yP_{1-x-y}$

PACS: 31.15.A–, 64.70.kd, 64.70.kg **DOI:** 10.1088/1674-1056/26/1/017303

1. Introduction

III–V semiconductor compounds have many advantages in the technology of modern optoelectronic devices[1] due to their specific electronic and optical properties and can be used in a very wide application field, including high-frequency electronic devices in modern communication systems such as mobile phones, high-speed optoelectronics and solar cells.[2,3]

Recently the electronic and optical properties of III–V binary semiconductors and their alloys have aroused great interest[4–13] because of their direct band gaps and high refractive indices, which give this kind of interesting semiconductor applications in optoelectronic and photovoltaic devices as well as widespread utilities in the fabrication of high-efficiency solar cells. The large breakdown fields, high thermal conductivities and electron transport properties of III–V nitrides such as GaN, InN and AlN make them suitable for novel optoelectronic applications in the visible and ultraviolet spectral range.[14]

Theoretical and experimental research has revealed an interesting property of InAs, InN and InP binary compounds that makes them very important materials in developing new technologies; hence, their ternary and quaternary alloys are expected to be very high-potential materials. Theoretical studies of these alloys offer the possibility of adapting parameters to obtain new materials with desired properties. $InAs_xN_yP_{1-x-y}$ triangular quaternary alloys are formed by three binary compounds: indium arsenide (InA), indium nitride (InN) and indium phosphide (InP), which are III–V semiconductors with a zinc blende structure at equilibrium.[15,16]

The aim of this work is to investigate the structural, electronic and optical properties of $InAs_xN_yP_{1-x-y}$ quaternary alloys using the full potential linearized augmented plane wave (FP-LAPW) method based on density functional theory (DFT), as implemented in the Wien2k code.[17]

First, the structural and electronic properties of binary compounds were investigated and our results showed good agreement with the available data in the literature. Second, the structural properties, the lattice constants, and the bulk modulus and its first pressure derivative were computed for different ternary and quaternary alloys, and the direct and indirect band gap energy as well as the density of state (DOS) were also computed and plotted. Moreover, we studied the optical properties and investigated the dielectric constants, refractive index and energy loss. To the best of our knowledge, this study is the first quantitative theoretical report of the fundamental physical properties of triangular $InAs_xN_yP_{1-x-y}$ quaternary alloys.

*Project supported by the Deanship of Scientific Research at King Saud University Group (Grant No. PRG-1437-39).
†Corresponding author. E-mail: abdiche_a@yahoo.fr
‡Corresponding author. E-mail: khenata_rabah@yahoo.fr
© 2017 Chinese Physical Society and IOP Publishing Ltd

2. Computational details

In this work, calculations were effectuated within the first-principles study using the Wien2k code based on the density functional theory (DFT). A non-relativistic full potential linearized augmented plane wave (FP-LAPW)[18] was applied.

Structural properties were handled using three different approximations for the exchange and correlation: the generalized gradient approximation of Wu and Cohen[19] (WC-GGA); Perdew–Burke–Ernzerhof (PBEsol-GGA);[20] and the local density approach (LDA). The results were fitted using Birch–Murnaghan's equation of state.[21] The band structure was calculated within the Tran–Blaha modified Becke–Johnson with the parameterization of Koller *et al.*[22]

For the total and partial densities of states (DOS), we considered In ($1s^2$ $2s^2$$2p^6$ $3s^2$ $3p^6$$3d^{10}$ $4s^2$ $4p^6$), As ($1s^2$ $2s^2$ $2p^6$ $3s^2$ $3p^6$ $3d^{10}$), N ($1s^2$) and P ($1s^2$ $2s^2$ $2p^6$) to be inner-shell electrons from the valence electrons of In ($4d^{10}$ $5s^2$ $5p^1$), As ($4s^2$ $3d^{10}$ $4p^3$), N ($2s^2$ $2p^3$) and P ($3s^2$ $3p^3$) shells.

We set the parameter $R_{\rm mt} \times K_{\rm max}$ equal to 8, whereas the muffin tin radii of In, As, N and P are set to 2.1, 1.9, 1.4, and 1.7, respectively. The integrals over the Brillouin zone are taken up to $72k$ points for binary compounds and $47k$ points for ternary and quaternary alloys for a chosen supercell of 8 atoms $1 \times 1 \times 1$.

3. Results and discussion

3.1. Structural properties

The $InAs_xN_yP_{1-x-y}$ triangular quaternary alloys are bounded by three ternary alloys, $InAs_xN_{1-x}$, $InAs_xP_{1-x}$, and InN_xP_{1-x}, which are delimited in their turn by three binary compounds, InAs, InN, and InP.

We used a single cell of eight atoms to model $InAs_xN_yP_{1-x-y}$ (x and $y = 0$, 0.25, 0.50, 0.75, 1). The structural properties, such as the lattice constants, the bulk modulus and its first-order pressure derivative, were computed for binary, ternary and quaternary alloys within the (WC-GGA), (PBEsol-GGA) and (LDA) approximations and fitted to Birch–Murnaghan's equation. The results for the binary constituents and the ternary and quaternary compounds are summarized in Tables 1 and 2, respectively.

Table 1. The lattice constants (a), bulk modulus (B) and the pressure derivative of the bulk modulus (B') for the InN, InPInAs, and their related zinc blende ternary alloys.

Composition x	Parameters	This work			Other theoretical studies	Experimental data
		WC-GGA	PBEsol-GGA	PW-LDA		
InN	a/Å	4.9926	4.9918	4.9471	4.945[a], 4.98[b]	4.98[f]
	B/GPa	140.5343	137.2588	145.5469	145[a], 155.35[b]	137[e]
	B'	4.1757	3.7960	3.6884	4.75[c], 4.49[b]	
InP	a/Å	5.8814	5.8789	5.8299	5.72[d], 5.85[g]	5.86[d]
	B/GPa	67.7383	67.2997	71.0719	73.66[d], 76.10[h]	72.00[d]
	B'	4.3041	4.5021	4.6221	4.20[i]	4.80[i]
InAs	a/Å	6.0898	6.0876	6.0298	5.9019[j]	6.0583[j]
	B/GPa	56.5406	56.3133	60.3092	61.90[j]	57.90[j]
	B'	4.0185	4.112	3.6884	4.487[j]	4.79[j]
$InN_{0.5}P_{0.5}$	a/Å	5.5052	5.5036	5.4525		
	B/GPa	84.1868	83.7418	92.0391		
	B'	4.5969	4.5467	4.3859		
$InAs_{0.5}P_{0.5}$	a/Å	5.9882	5.9864	5.9321	5.997[k], 6.081[k]	
	B/GPa	61.2399	61.0632	65.3308	60.82[k],	
	B'	4.6824	4.7091	4.6646	52.86[k]	
$InAs_{0.5}N_{0.5}$	a/Å	5.6432	5.6408	5.5833		
	B/GPa	73.9522	74.1169	80.106		
	B'	4.041	3.8789	4.6129		

[a]Ref. [28], [b]Ref. [29], [c]Ref. [30], [d]Ref. [31], [e]Ref. [32], [f]Ref. [33], [g]Ref. [34], [h]Ref. [35], [i]Ref. [36], [j]Ref. [37], and [k]Ref. [38].

Table 2. The lattice constants (a), bulk modulus (B) and pressure derivative of the bulk modulus (B') for the zinc blende quaternary alloys.

Composition x	Parameters	This work			Other theoretical studies	Experimental data
		WC-GGA	PBEsol-GGA	PW-LDA		
$InAs_{0.25}N_{0.25}P_{0.5}$	a/Å	5.7717	5.7697	5.7153		
	B/GPa	69.0549	68.9951	71.548		
	B'	4.774	4.72	3.6102		
$InAs_{0.25}N_{0.5}P_{0.25}$	a/Å	5.5763	5.5732	5.5198		
	B/GPa	77.3433	76.0968	88.9881		
	B'	3.922	3.7396	3.9196		
$InAs_{0.5}N_{0.25}P_{0.25}$	a/Å	5.8316	5.8300	5.7735		
	B/GPa	64.0390	64.6417	70.8649		
	B'	3.8116	4.0499	4.5821		

The calculated equilibrium lattice constants and bulk modulus for the $InAs_xN_{1-x}$, $InAs_xP_{1-x}$, and InN_xP_{1-x} ternary alloys are plotted as functions of composition x in Figs. 1 and 2, respectively. The results show that the lattice parameter increases with the increase of the$x$ composition for $InAs_xN_{1-x}$ and $InAs_xP_{1-x}$ but decreases in the case of InN_xP_{1-x}. For $InAs_xN_{1-x}$ and $InAs_xP_{1-x}$, we found a volume expansion due to the atomic radius of As, whereas we observe a volume compression in the case of InN_xP_{1-x} due to the introduction of the nitride atom N. We note that the lattice constant and bulk modulus are proportional: $D \propto V_0^{-1}$.[23] Otherwise, the lattice mismatch for InAs, InN, and InP would cause a slight deviation from Vegard's law.[24]

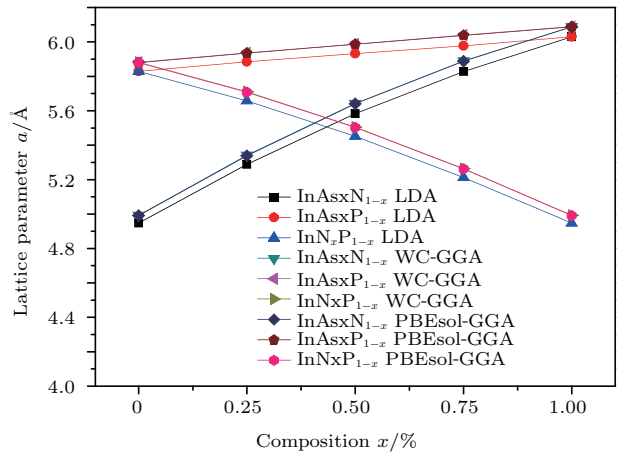


Fig. 1. (color online) Variation of the lattice constant versus composition x of the (ZB) InN_xP_{1-x}, $InAs_xN_{1-x}$ and $InAs_xP_{1-x}$ ternary alloys.

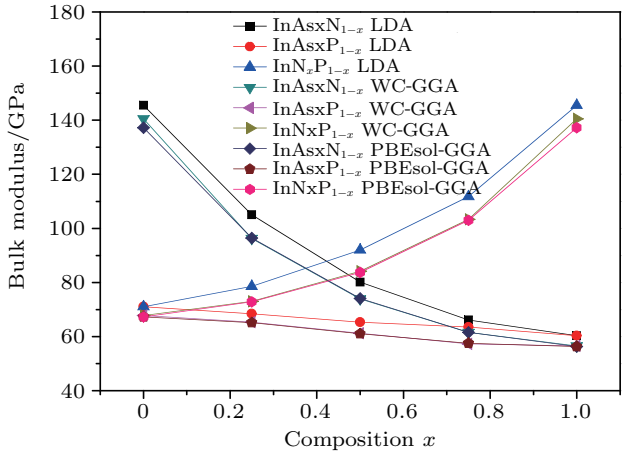


Fig. 2. (color online) Variation of bulk modulus versus composition x of the (ZB) InN_xP_{1-x}, $InAs_xN_{1-x}$ and $InAs_xP_{1-x}$ ternary alloys.

The calculated values were fitted with a simple quadratic polynomial function given in the following formulas:

$$a(x) = xa_{\mathrm{InAs}} + (1-x)a_{\mathrm{InP}} - x(1-x)b, \quad (1)$$

$$a(x) = xa_{\mathrm{InAs}} + (1-x)a_{\mathrm{InN}} - x(1-x)b, \quad (2)$$

$$a(x) = xa_{\mathrm{InN}} + (1-x)a_{\mathrm{InP}} - x(1-x)b, \quad (3)$$

where a_{InAs}, a_{InP}, and a_{InN} are the lattice parameters of InAs, InP, and InN binary compounds respectively b is the bowing parameter of the lattice constant. The bulk modulus bowing parameters were calculated in the same scheme.

For the quaternary alloys, the variations in the lattice parameters and bulk modulus versus compositions x and y are summarized in Table 2 and depicted in Figs. 3 and 4. The triangular behavior of our quaternary alloys is due to its definition set $(1-x-y \geq 0)$ for compositions x and y, which includes only three (x, y) pairs: (0.25, 0.25), (0.25, 0.50) and (0.50, 0.25). This combination gives us three quaternary compounds: $InAs_{0.25}N_{0.25}P_{0.5}$, $InAs_{0.25}N_{0.50}P_{0.25}$, and $InAs_{0.50}N_{0.25}P_{0.25}$. We also note the increase in the lattice constant with the arsenic composition increasing and a decrease with the nitride fraction increasing, which are clearly due to the atomic radius. There is inverse variation with the bulk modulus, which confirms the relationship between the bulk modulus and lattice constants.

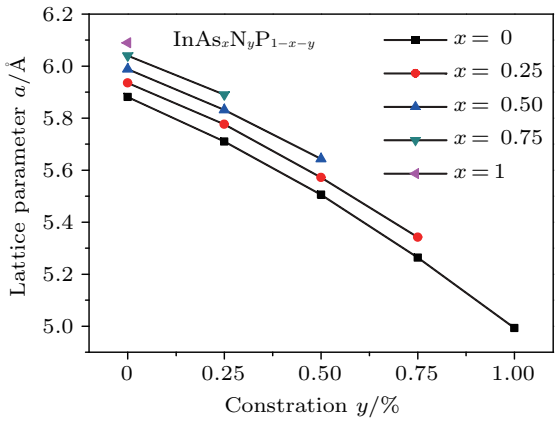


Fig. 3. (color online) Variation of the lattice constant versus compositions x and y of the (ZB) $InAs_xN_yP_{1-x-y}$ quaternary alloys.

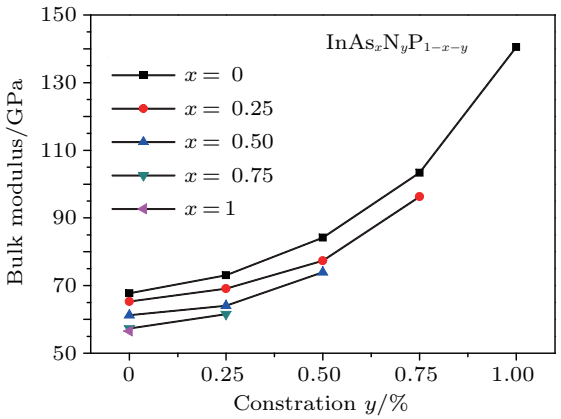


Fig. 4. (color online) Variation of bulk modulus versus compositions x and y of the (ZB) $InAs_xN_yP_{1-x-y}$ quaternary alloys.

Furthermore, we calculated the formation energy $E_{\mathrm{form}}(x,y)$ of the quaternary alloys using

$$E_{\mathrm{form}}(x,y) = E_{\mathrm{InAsNP}}(x,y) - xE_{\mathrm{InAs}}$$

$$-yE_{\mathrm{InN}}-(1-x-y)E_{\mathrm{InP}}, \quad (4)$$

where E_{InAs}, E_{InN}, and E_{InP} are the total energies of the corresponding binary compounds.

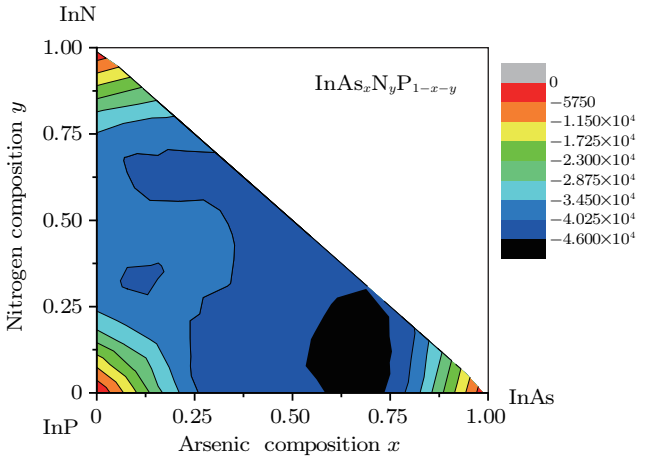


Fig. 5. (color online) Contour map of the calculated forming energy versus composition of zinc blende $InAs_xN_yP_{1-x-y}$ quaternary solid solutions.

The variations in the formation energies are shown in a contour plot in Fig. 5. It is clearly seen that our alloys have a higher chance to be formed at the corner zones on the graph, the more one moves away from the corners, the formation becomes more difficult. Materials formed in the darker zone close to a 60% concentration of arsenic are the least stable materials. The energies obtained are negative, which means that our alloys can be formed for all compositions considered.

3.2. Electronic properties

3.2.1. Band structures

For binary and ternary alloys, the values of the band gap energies of the direct and indirect transitions were calculated using the Tran–Blaha modified Becke–Johnson (TB-mBJ) approach and are listed together with the data available in theoretical and experimental works in Table 3.

Table 3. The band gap energies of the direct and indirect transitions of the InN, InPInAs and their related zinc blende ternary alloys, where the values are given in eV.

Composition x at P atom	Band gap energy /eV	This work LDA_mBJ	Other theoretical studies	Experimental data
InN	$E_{\Gamma\to\Gamma}$	0.79110	0:69[a]	0.7[c]
	$E_{\Gamma\to X}$	4.06859	2.765[b]	2:11[d]
InP	$E_{\Gamma\to\Gamma}$	1.66753	1.423[e]	1.35[f]
	$E_{\Gamma\to X}$	2.36479	1.63[g]	2.21[f]
InAs	$E_{\Gamma\to\Gamma}$	0.68182	0.568, 0.499	
	$E_{\Gamma\to X}$	2.19368		
$InN_{0.5}P_{0.5}$	$E_{\Gamma\to\Gamma}$	0.87223		
	$E_{\Gamma\to X}$	3.35265		
$InAs_{0.5}P_{0.5}$	$E_{\Gamma\to\Gamma}$	1.1964	1.036, 0.766	
	$E_{\Gamma\to X}$	2.8897		
$InAs_{0.5}N_{0.5}$	$E_{\Gamma\to\Gamma}$	0.45203		
	$E_{\Gamma\to X}$	3.30711		

[a]Ref. [39], [b]Ref. [29], [c]Ref. [33], [d]Ref. [40], [e]Ref. [41], [f]Ref. [42], [g]Ref. [36].

We plotted the variations of the direct and indirect band gap versus the composition x of InNP, InAsN and InAsP ternary alloys (Fig. 6). The results show that our ternary alloys have a direct band gap for each composition x, and confirmed the importance of these materials in optoelectronic technology.

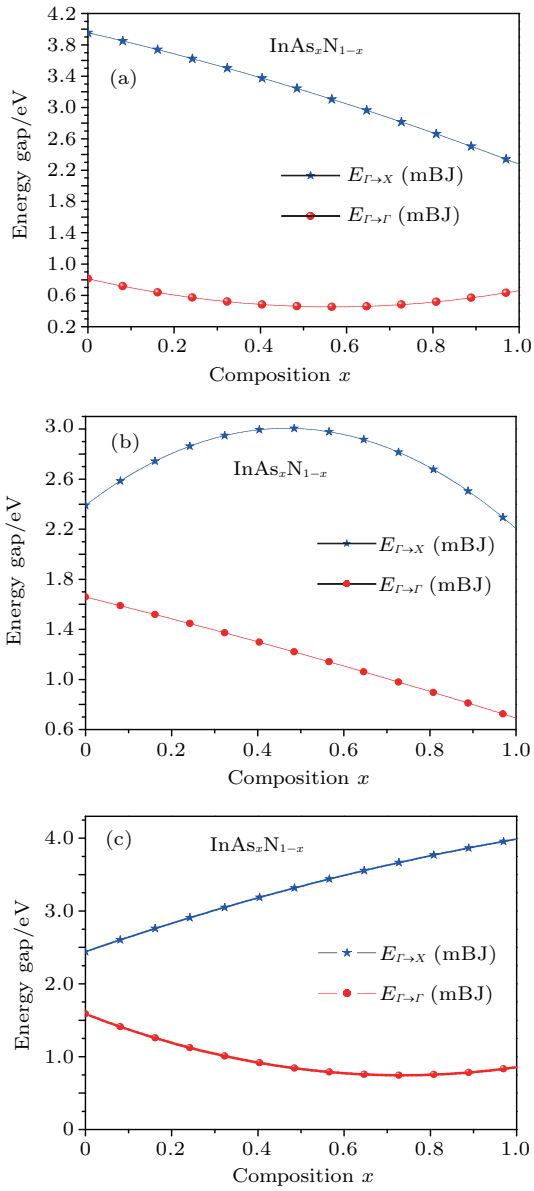


Fig. 6. (color online) The variations curves versus composition x of each band gap ($E_{\Gamma\to\Gamma}$, $E_{\Gamma\to X}$) of the InN_xP_{1-x} (a), $InAs_xN_{1-x}$ (b), and $InAs_xP_{1-x}$ (c) ternary alloys.

Moreover, the computed values of the band gap are fitted to a quadratic polynomial, where the bowing factors of the direct energy band gap are found to be equal to 1.56, 1.11, and –0.12 for InN_xP_{1-x}, $InAs_xN_{1-x}$, and $InAs_xP_{1-x}$ respectively.

The equations of the fitted curves are as follows:

For InN_xP_{1-x}:

$$E_{\Gamma\to\Gamma}=1.587-2.2936x+1.5625x^2, \quad (5)$$

$$E_{\Gamma\to X}=2.4411+2.0475x-0.5007x^2. \quad (6)$$

For $InAs_xN_{1-x}$:

$$E_{\Gamma\to\Gamma} = 0.81 - 1.26x + 1.11x^2, \quad (7)$$

$$E_{\Gamma\to X} = 3.95 - 1.27x - 0.4x^2. \quad (8)$$

For $InAs_xP_{1-x}$:

$$E_{\Gamma\to\Gamma} = 1.65 - 0.84x - 0.12x^2, \quad (9)$$

$$E_{\Gamma\to X} = 2.39 + 2.63x - 2.81x^2. \quad (10)$$

For the band gap structure of $InAs_xN_yP_{1-x-y}$ quaternary alloys, the direct and indirect band gap energies were computed using the best approach TB-mBJ with the parameterization of Koller *et al.* The band structures are presented in Figs. 7(a)–7(c) for $InAs_{0.25}N_{0.25}P_{0.50}$, $InAs_{0.25}N_{0.50}P_{0.25}$, and $InAs_{0.50}N_{0.25}P_{0.25}$, respectively. Our calculations show that these materials are semiconductors with direct band gaps of approximately 0.78 eV, 0.65 eV, and 0.61 eV for $InAs_{0.25}N_{0.25}P_{0.50}$, $InAs_{0.25}N_{0.50}P_{0.25}$, and $InAs_{0.50}N_{0.25}P_{0.25}$, respectively. The calculated values for the direct and indirect band gap energies are summarized in Table 4 and plotted as functions of compositions x and y in Figs. 8 and 9. The figures show the nonlinear behavior of each band gap and the decrease of the direct band gap versus composition: at a fixed composition x, the direct band gap energies decrease with y composition increasing. The indirect band gap energies increase with y composition increasing at a fixed composition x. The lowest value observed is 0.452 eV, which corresponds to the composition of 50% arsenic (As) and 50% nitride (N). These compositions correspond to the ternary $InAs_{0.5}N_{0.5}$ alloy. The higher value is found to be equal to 1.19 eV and corresponds to the ternary $InAs_{0.5}P_{0.5}$ compound.

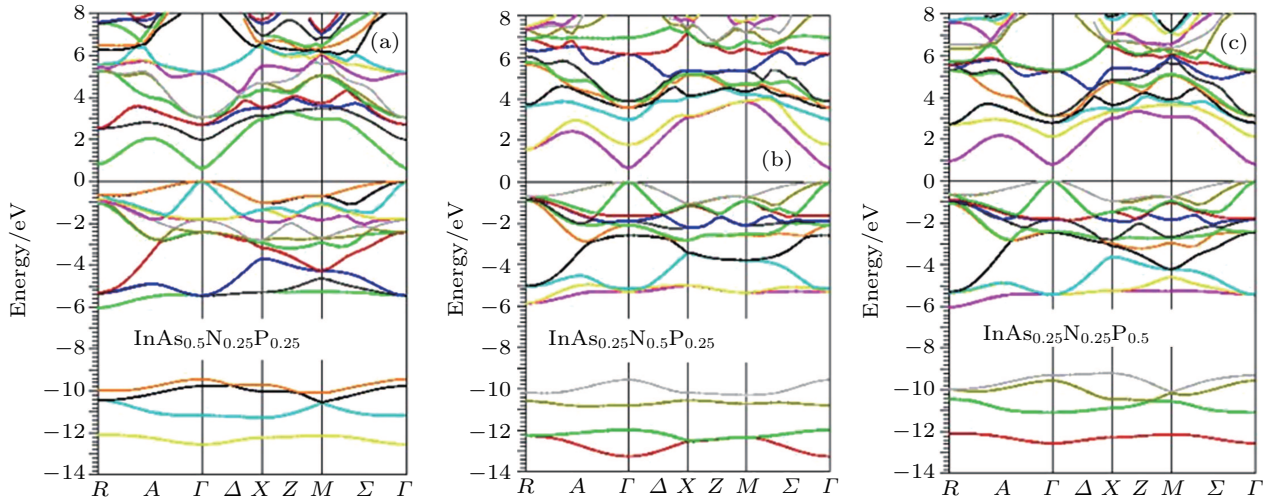


Fig. 7. (color online) The electronic band structures of the cubic (a) $In\,As_{0.50}N_{0.25}P_{0.25}$, (b) $In\,As_{0.25}N_{0.50}P_{0.25}$, and (c) $In\,As_{0.25}N_{0.25}P_{0.50}$ quaternary alloys within TB-mBJ approximation.

Table 4. The band gap energies of the direct and indirect transitions of the zinc blende quaternary alloys, where the values are given in eV.

Composition x at P atom	Band gap energy/ eV	This work		Other theoretical studies	Experimental data
		LDA	LDA_mBJ		
$InAs_{0.25}N_{0.25}P_{0.5}$	$E_{\Gamma\to\Gamma}$	0.00792	0.78529		
	$E_{\Gamma\to X}$	2.26488	2.99961		
$InAs_{0.25}N_{0.50}P_{0.25}$	$E_{\Gamma\to\Gamma}$	0.0000	0.65339		
	$E_{\Gamma\to X}$	2.36104	3.11918		
$InAs_{0.50}N_{0.25}P_{0.25}$	$E_{\Gamma\to\Gamma}$	0.0000	0.61100		
	$E_{\Gamma\to X}$	2.27110	2.97629		

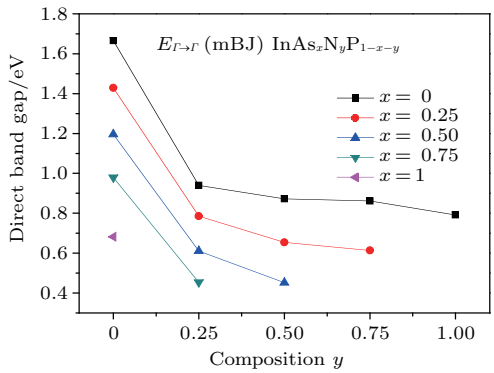


Fig. 8. (color online) The variation curves versus compositions x and y of the direct band gap ($E_{\Gamma\to\Gamma}$) of $InAs_xN_yP_{1-x-y}$ quaternary alloys.

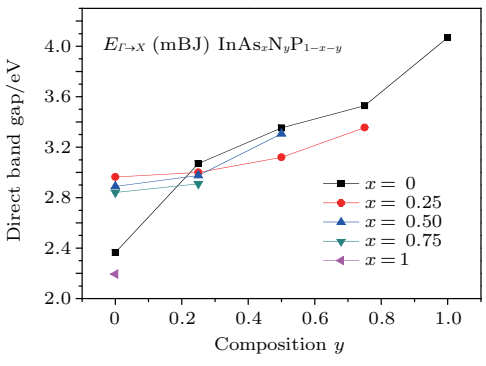


Fig. 9. (color online) The variation curves versus compositions x and y of the indirect band gap ($E_{\Gamma\to X}$) of $InAs_xN_yP_{1-x-y}$ quaternary alloys.

It is important to note that we have not found any previous works in the literature regarding the triangular $InAs_xN_yP_{1-x-y}$ quaternary alloys, making this work a first prediction to be verified by future experimental and theoretical studies.

3.2.2. Density of states

To confirm the calculated band structures, we computed the total and partial densities of states for the quaternary $InAs_{0.25}N_{0.25}P_{0.5}$, $InAs_{0.25}N_{0.5}P_{0.25}$, and $InAs_{0.5}N_{0.25}P_{0.25}$ alloys.

The results are shown in Fig. 10, which reveals the compatibility with the band structures. The density of states may be divided into three distinct regions: the conduction band (CB) results from a mixture of As-5p, N-2P and P-3p states, and the valence band (VB) comprises a lower (LVB) and an upper (UVB) band, where the lower band (LVB) consists mainly of In-4d states with a mixture of As-5s, N-2s and P-3s and the upper band (UVB) is dominated by the In-5s state with a small contribution the of As-5p, N-2p and P-3p states. For all quaternary alloys, a consistent contribution from the same orbital is observed, except for an upward trend in magnitude related to the values of x and y.

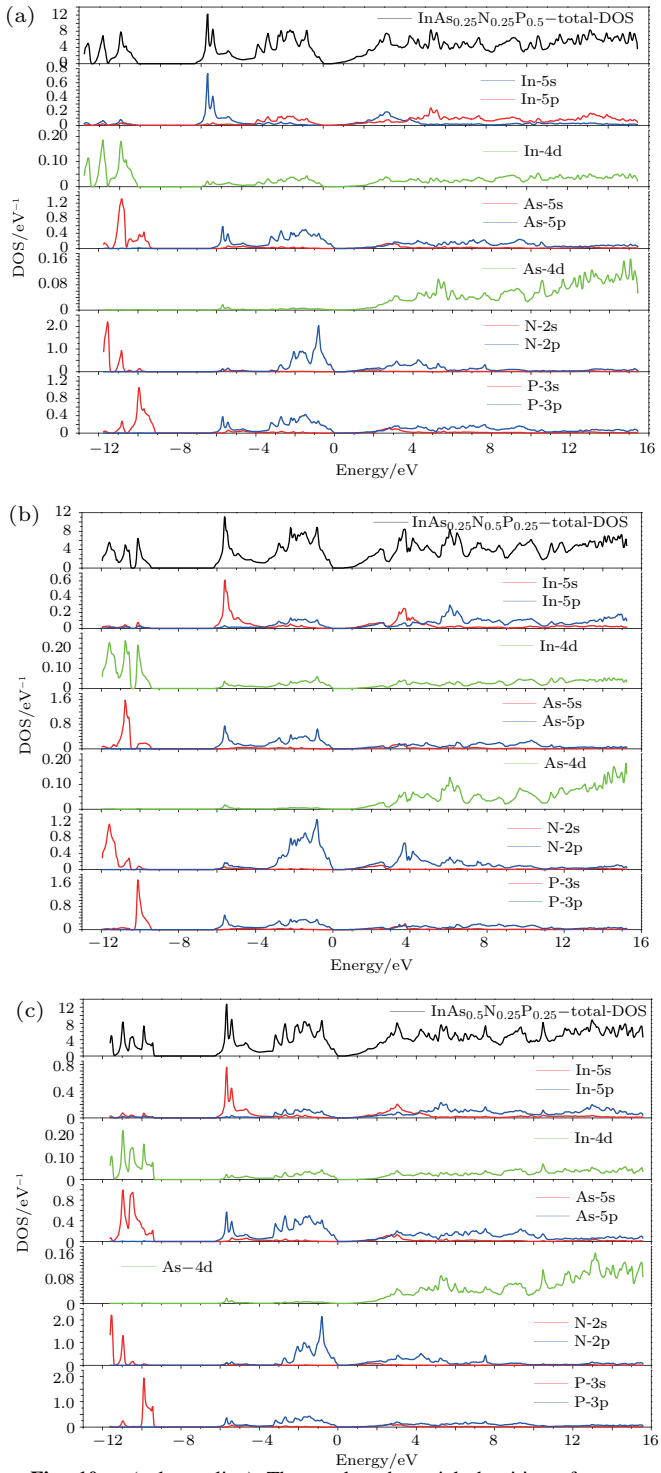


Fig. 10. (color online) The total and partial densities of states (DOSs) for (a) $InAs_{0.25}N_{0.25}P_{0.5}$, (b) $InAs_{0.25}N_{0.5}P_{0.25}$, and (c) $InAs_{0.5}N_{0.25}P_{0.25}$ alloys, respectively.

3.3. Optical properties

The optical properties of $InAs_xN_yP_{1-x-y}$ quaternary alloys, such as the dielectric function with its real and imaginary parts, the refractive index and the loss energy, were computed and plotted in Figs. 11–13, respectively.

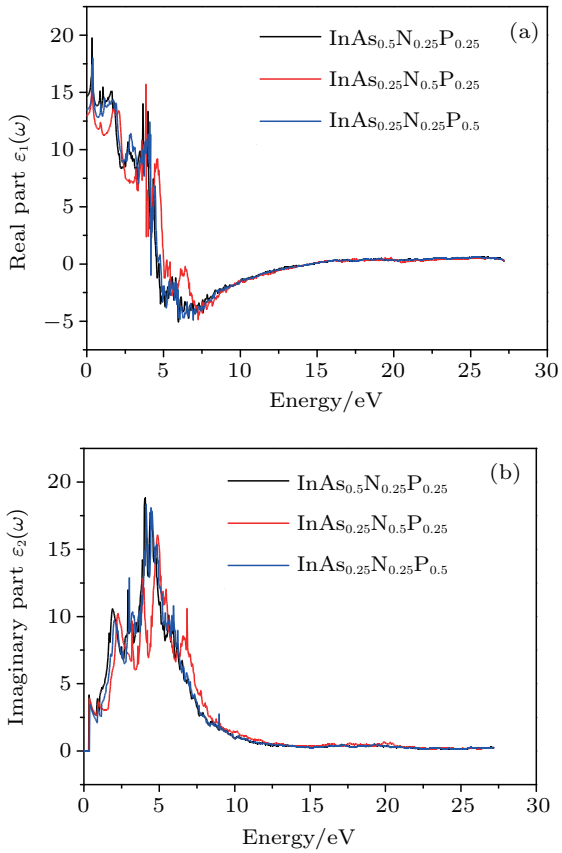


Fig. 11. (color online) The real parts (a) and imaginary parts (b) of the dielectric function of $InAs_{0.25}N_{0.25}P_{0.5}$, $InAs_{0.25}N_{0.5}P_{0.25}$, and $InAs_{0.5}N_{0.25}P_{0.25}$ quaternary alloys.

The frequency-dependent dielectric functions $\varepsilon_1(\omega)$ and $\varepsilon_2(\omega)$[25] the real and imaginary parts of the complex dielectric function $\varepsilon\omega$), respectively, are given by the following

equations:

$$\varepsilon_2(\omega) = \frac{e^2\hbar}{\pi m^2\omega^2}\sum_{v,c}\int_{zB}|M_{cv}(k)|^2\,\delta\left[\omega_{cv}(k)-\omega\right]\mathrm{d}^3k, \quad (11)$$

$$\varepsilon_1(\omega) = 1+\frac{2}{\pi}P\int_0^{\infty}\frac{\omega'\varepsilon_2(\omega')}{\omega'^2-\omega^2}\mathrm{d}\omega'. \quad (12)$$

In the imaginary part $\varepsilon_2(\omega)$, the momentum dipole elements

$$M_{cv}(k) = \langle u_{vk}|\boldsymbol{\delta}\nabla|u_{ck}\rangle, \quad (13)$$

describe the direct transitions between the valence and the conduction band u_{vk} and u_{ck} states, respectively, with $\boldsymbol{\delta}$ as a unit vector defining the electric field. The integral is taken over the first Brillouin zone. In the real part $\varepsilon_1\omega$, P indicates that the integral is to be evaluated in the principal value sense. This value can be calculated from the imaginary part using the Kramers–Kronig transformation.[26]

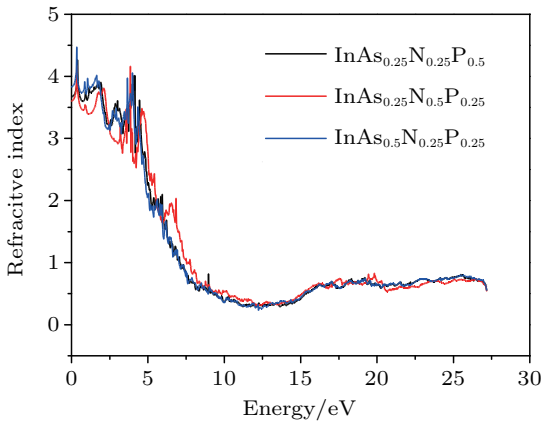


Fig. 12. (color online) The refractive indexes of $InAs_{0.25}N_{0.25}P_{0.5}$, $InAs_{0.25}N_{0.5}P_{0.25}$, and $InAs_{0.5}N_{0.25}P_{0.25}$ quaternary alloys.

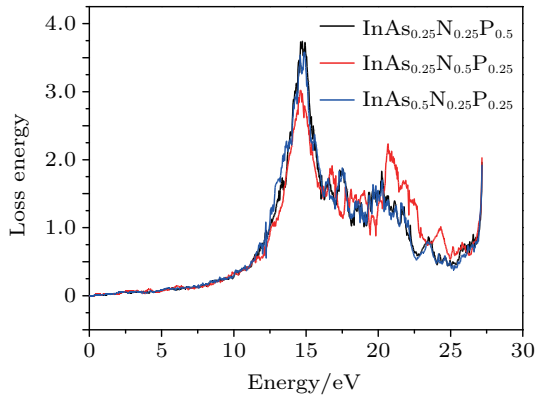


Fig. 13. (color online) Energy loss of $InAs_{0.25}N_{0.25}P_{0.5}$, $InAs_{0.25}N_{0.5}P_{0.25}$ and $InAs_{0.5}N_{0.25}P_{0.25}$ quaternary alloys.

Moreover, we calculated the refractive index $n(\omega)$ using the dielectric function, given by the following expression

$$n(\omega) = \left[\frac{\varepsilon_1(\omega)}{2}+\frac{\sqrt{\varepsilon_1^2(\omega)+\varepsilon_2^2(\omega)}}{2}\right]^{1/2}. \quad (14)$$

Other models were used to calculate the refractive index $n(\omega)$ to compare and confirm the results. These models are presented as follows:

Moss model:[27]

$$n^4E_g = 95\ \mathrm{eV}, \quad (15)$$

where n and E_g are the refractive index and the energy gap, respectively.

Ravindra relation:[27]

$$n = 4.084 - 0.62E_g. \quad (16)$$

Herve–Vandamme relation:[27]

$$n^2 = 1+\left(\frac{A}{E_g+B}\right)^2, \quad (17)$$

where A is the hydrogen ionization energy 13.6 eV and $B = 3.47$ eV is a constant presumed to be the difference between the UV resonance energy and the band gap E_g.

Reddy relation:[27]

$$n^4(E_g-0.365) = 154. \quad (18)$$

The curves in Figs. 11–13 show the similarity of the spectra, except for a slight shift explained by the effects of the variation of the nitride and arsenide concentrations (x,y) on the band energies.

In the imaginary part of the dielectric function displayed in Fig. 11(b), the absorptions of materials are visible in the main peaks at approximately 18.79, 17.72, and 16.1, at energies of approximately 4.06 eV, 4.39 eV, and 5.91 eV, respectively. These peaks may belong to the direct electronic transition from the top of the valence bands to the bottom of the conduction bands in the direction $\Gamma\rightarrow\Gamma$, which is known as the fundamental absorption edge. The real parts of the dielectric function for the considered compounds are shown in Fig. 11(a). The imaginary parts increase and present major peaks at low energy: the peaks are located at the energy of 0.4 eV and decrease with the increase of the energy, along with the appearance of some small peaks.

Figure 12 shows the refractive index $n\omega$ curves of the $InAs_{0.25}N_{0.25}P_{0.5}$, $InAs_{0.25}N_{0.5}P_{0.25}$, and $InAs_{0.5}N_{0.25}P_{0.25}$ quaternary alloys. The static values of the refractive index $n(0)$ were computed using the real part of the dielectric function $\varepsilon_1\omega$) and show excellent agreement with the values calculated using different models presented in Eqs. (15)–(18). The calculated values are summarized in Table 5.

Overall, the optical constants of $InAs_xN_yP_{1-x-y}$ alloys change slightly with nitride and arsenide compositions. The loss function spectra presented in Fig. 13 describe the energy loss of a fast electron traversing the alloys. We observe from this figure that for a photon with energy less than the band gap of the considered compound, no energy loss occurs, which means that no scattering occurs. The peaks at approximately 14.8, 16.5, and 17.5 in the loss function are plasma resonance peaks and are the points of the transition from a metallic to dielectric character.

Table 5. Calculated refractive index $n(\omega)$ of InAsNP quaternary alloys.

Compound	FP-LAPW $n(\omega=0)$	Herve–Vandam $n(\omega=0)$	Ravindra $n(\omega=0)$	Reddy $n(\omega=0)$	Moss $n(\omega=0)$
$InAs_{0.25}N_{0.25}P_{0.5}$	3.6	3.35	3.6	3.6	3.32
$InAs_{0.25}N_{0.50}P_{0.25}$	3.69	3.44	3.6	3.8	3.47
$InAs_{0.50}N_{0.25}P_{0.25}$	3.85	3.48	3.7	3.9	3.53

4. Conclusions

In this paper, we studied the structural, electronic, and optical properties of the $InAs_xN_yP_{1-x-y}$ quaternary solid solutions. The results can be summarized as follows.

(I) We obtained different values of lattice constants, which offer the possibility of deposition on different substrates such as InP and GaAs.

(II) The band gap varies in a large band situated between 045 eV and 119 eV, which enlarges the application domain.

(III) The quaternary alloys can be formed in the range of compositions considered.

(IV) Optical stability is not affected by the changes in the compositions of nitride and arsenide.

References

[1] Smokal V, Derkowska B and Czaplicki R 2009 *Opt. Mater.* **31** 518
[2] Chen A B and Sher A 1980 *Phys. Rev. B* **23** 5360
[3] Shimomura A, Anan T and Sugou S 1996 *J. Cryst. Growth* **162** 121
[4] Johnson N F, Ehrenreich H, Hui P M and Young P M 1990 *Phys. Rev. B* **41** 3655
[5] Reshak A H 2006 *J. Chem. Phys* **125** 034710
[6] Al-Douri Y and Reshak A H 2011 *Appl. Phys. A* **104** 1159
[7] Bredin J L 1994 *Science* **263** 487
[8] Borak A 2005 *Science* **308** 638
[9] Levine J Hand Allan D C 1991 *Phys. Rev. Lett.* **66** 41
[10] Reshak A H and Auluck S 2007 *Physica B* **395** 143
[11] Reshak A H 2005 *Eur. Phys. J. C* **47** 503
[12] Tit N, Amrane N and Reshak A H 2010 *Cryst. Res. Technol.* **45** 59
[13] Haq B U, Ahmed R, Hassan F E H, Khenata R, Kamin M K and Goumri S 2014 *Solar Energy* **100** 1
[14] Kasap S and Cappers P (Eds.) 2006 *Springer Handbook of Electronics and Photonic Materials* (Springer)
[15] Wang Y, Yin H, Cao R, Zahid F, Zhu Y, Liu L, Wang J and Guo H 2013 *Phys. Rev. B* **87** 235203
[16] Marvin L, James C and Chelikowsky R *Electronic Structure and Optical Properties of Semiconductors* (in *Springer Series in Solid-State Sciences* Vol. 75) pp. 79–139
[17] Blaha P, Schwarz K, MadsenG K H, Kvasnicka D and Luitz J 2001 *Wien2k, An Augmented Plane Wave Plus Local Orbital Program for Calculating Crystal Properties* (Vienna: Vienna University of Technology)
[18] Schwarz K and Blaha P 2003 *Comput. Mater. Sci.* **28** 266
[19] Wu Z and Cohen R E 2006 *Phys. Rev. B* **73** 235116
[20] Perdew J P, Burke K and Ernzerhof M 1996 *Phys. Rev. Lett.* **77** 3865
[21] Murnaghan F D 1944 *Proc. Natl. Acad. Sci. USA* **30** 244
[22] Koller D, Tran F and Blaha P 2012 *Phys. Rev. B* **85** 1
[23] Guemou M, Bouhafs B, Abdiche A, Khenata R, Al Douri Y and Bin O S 2012 *Physica B* **407** 1292
[24] Vegard L 1921 *Zeitschrift Fur Physik* **5** 17
[25] Adachi S 2009 *Properties of Semiconductor Alloys: Group-IV, III–V and II–VI Semiconductors*(John Wiley & Sons)
[26] Ouahrani T, Reshak A H, Khenata R, Amrani B, Mebrouki M, Otero-de-la Roza A and Luana V 2010 *J. Solid State Chem.* **183** 46
[27] Tripathy S 2015 *Opt. Mater.* **46** 240
[28] Shi H and Duan Y 2008 *Phys. Lett A* **373** 165
[29] Abdiche A, Abid H, Riane R and Bouaza A 2010 *Acta Phys. Polonica* **117** 921
[30] Ziane M I, Zouaoui B, Ouahrani T and Hamza B 2015 *Mater. Sci. Semicond Process* **30** 181
[31] Ben F J, Debbichi M and Said M 2007 *Microelectronic J.* **38** 860
[32] Serrano J, Rubio A Hernandez E, Munoz A and Mujica A 2000 *Phys. Rev. B* **62** 16612
[33] Ahmed R, Hashem far S J, Akbarzadeh H, Ahmed M and Aleem F 2007 *Computat. Mater. Sci.* **39** 580
[34] Wang S Q and Yes H Q 2002 *Phys. Rev. B* **66** 235111
[35] Hellwege K H Madelung O, Landolt H and Bornstein R 1982 *Semiconductors: Physics of Group IV Elements and III–V Compounds* (New Series, Group III, 17a) (Berlin: Springer Verlag) p. 602
[36] Shen W and Zunger A 1999 *Phys. Rev. B* **60** 5404
[37] van Camp P E, van Doren V E and Devreese J T 1990 *Phys. Rev. B* **41** 1598
[38] Nemiri O, Ghemid S, Chouahda Z, Meradji H and El Haj H F 2013 *Int. J. Mod. Phys. B* **27** 1350166
[39] Bechstedt F and Del Sole R 1988 *Phys. Rev. B* **38** 7710
[40] Edgar J H 1994 Properties of Group III-Nitrides *EMIS Data Reviews* 11, *INSPEC*, London, p. 10233
[41] Rochon P and Fortin E 1975 *Phys. Rev. B* **12** 5803
[42] Madelung O, Schulz M, Londolt H and Bornstein R 1987 *Numerical Data and Functional Relationships in Science and Technology in Cryst. Solid State Phys.* 17 (Berlin: Springer Verlag)